Creep tests with frozen soils under uniaxial tension and uniaxial compression

H. ECKARDT

Centre d'ingénierie nordique, École Polytechnique, Campus de l'Université de Montréal, C.P. 6079, Succ. A, Montréal, Québec, Canada H3C 3A7

Test equipment, test procedure, and test results of uniaxial creep tests under compression and tension are presented. The material used, was a medium grain-size sand and a clayey, sandy silt. The compression tests were carried out on cylindrical samples with a ratio height to diameter of h/d = 20/10 cm. For tension tests, the sample was a dog-bone shaped specimen with a cylindrical part in the middle. The hight of this part was h = 15 cm and its diameter was d = 5 cm. Only that part was used for deformation measurements. The test results were obtained as creep curves and they show different creep behaviour under compression and tension within comparable conditions. The failure deformation under tension is much smaller than under compression where as the deformation rate under tension is higher than under compression. For both a granular and a cohesive soil, the samples showed qualitatively the same creep behaviour.

Describing the creep behaviour analytically, the frozen soil is taken as a continuum taking into account a restriction on constant volume deformation. The stress-strain behaviour, independent of dimensions, can be described by a power law, which contains a temperature and time dependent modulus. Creep parameters for this equation are evaluated from test results and a complete set of data is given for both types of soil. The parameters are different for the same soil under tension and under compression. Test and computation results as well as physical explanations of the different creep behaviour are discussed.

On traite dans la présente communication du matériel et de la méthode utilisés ainsi que des résultats obtenus lors d'essais de fluage uniaxial de sols soumis à des contraintes de compression et de traction. Les matériaux utilisés étaient un sable moyen et un limon sableux et argileux. Les essais de compression ont été effectués sur des échantillons cylindriques dont le rapport hauteur/diamètre, h/d, était 20/10 cm. Les échantillons utilisés pour les essais de traction avaient la forme d'os de chien ayant une partie centrale cylindrique. Cette partie centrale avait une hauteur h de 15 cm et un diamètre d de 5 cm. Les mesures de déformation ont été faites seulement sur cette partie. Les résultats obtenus ont été mis sous la forme de courbes de fluage révélant différentes caractéristiques de fluage en compression et en traction dans des conditions comparables. La déformation de rupture par traction est beaucoup plus faible que celle par compression alors que la vitesse de déformation par traction est plus grande que celle par compression. Qualitativement, les caractéristiques de fluage des échantillons de sol granulaire et celles des échantillons de sol cohérent sont les mêmes.

Dans la description analytique des caractéristiques de fluage, on considère le sol gelé comme un continuum, à l'exception de la déformation volumétrique constante. La relation contrainte-déformation, quelles que soient les dimensions, peut être décrite par une loi de puissance qui contient un module fonction de la température et du temps. On évalue les paramètres de fluage pour cette équation à partir des résultats d'essais et on donne un ensemble de données pour les deux types de sol. Un type de sol donné présente des paramètres différents selon qu'il est soumis à une traction ou à une compression. On présente les résultats des essais et des calculs ainsi que les explications physiques des différentes caractéristiques de fluage.

Proc. 4th Can. Permafrost Conf. (1982)

Introduction

When constructing excavations in naturally or artificially frozen grounds the soil in general can be loaded with earth- or water pressure like a concrete. This advantage and further developments of modern, artificial, ground freezing techniques have lead to complex applications of the ground freezing methods in civil engineering. It is used mainly in tunnelling, shaft constructions, and underpinnings. Some recent case studies can be found in the *Proceedings of the Second International Symposium on Ground Freezing* held in Trondheim, Norway in 1980. Taking advantage of the shape flexibility of frozen soil structures one usually gets combined states of stress within the structure depending on its shape and load.

Successful engineering treatment of those problems requires finding a safe, functional, and economical solution for the construction of a frozen ground structure in each particular case. To solve this problem means to know the mechanical properties of frozen soils. Those can be expressed by constitutive equations and creep laws describing the time independent and time dependent stress-strain behaviour for different states of stress and temperatures.

Up to now many tests *in situ* and in the laboratory have been performed to develop those constitutive equations. Most of these tests were performed as uniaxial or triaxial compression tests (Chamberlain *et al.* 1972; Sayles 1968) and the results are valid for those states of stresses and strains existing in the test.

For describing the complete deformation behaviour of a frozen soil structure under combined states of stress, the stress-strain behaviour under tension stresses must also be known. In the literature there are some results of tensile tests describing the time independent stress-strain behaviour of frozen soils (Zelenin *et al.* 1958) but only very few results are available about creep behaviour of frozen soils under tensile stresses (Grechishchev 1976).

The author found it necessary to perform pure uniaxial tensile tests under creep load when developing a method for calculating deformations of frozen soil retaining structures under bending load. In this paper, test equipment, test procedure, and test results of these uniaxial creep tests, under tension as well as under compression, are presented and discussed.

Experimental Tests

General

In order to get a good transfer from test results into practice, sample material, sample preparation, test procedure, and variable test parameters were chosen as close to reality as possible. The following ranges of parameters were found to be important for this investigation since they are derived from experiences with the freezing technique. They are lower and upper boundary conditions for the test equipment and in the test performance:

Temperature T :	$-40°C \leqslant T \leqslant -5°C$
Time under load t_B :	$1\,h \leqslant t_B \leqslant 10{,}000\,h$
Uniaxial stress σ_1 :	$-3{,}000\,kPa \leqslant \sigma_1 \leqslant$ 10,000 kPa, tens. neg.
Failure deformation ε_f :	$-2\% \leqslant \varepsilon_f \leqslant 7\%$
Deformation rate $\dot{\varepsilon}$:	$1.10^{-6}/h \leqslant \dot{\varepsilon} \leqslant 5.10^{-3}/h$.

All tests were performed in the cold rooms of the Institute of Soil Mechanics and Rock Mechanics of the University of Karlsruhe, West Germany. The temperature in these rooms was controlled with an accuracy of ± 0.5°C and the room temperatures corresponded to test temperatures. All kinds of measurements, i.e. temperature, deformation, and load, were measured mechanically as well as electronically with a good agreement between both systems.

Tests were performed on samples of a cohesive and a cohesionless soils. As a cohesionless soil, a medium grain-size sand was used with specifications given in Figure 1.

The dry sand in the mold had a void ratio of about $e = 0.5$ and its average density was about $\rho_d = 1750$ kg/m^3. All samples were water saturated before freezing.

As a cohesive soil, a clayey sandy silt was used with specifications given in Figure 2. The silt was filled in the mold with a water content above the liquid limit. Then a consolidation stress of $\sigma_v = 100$ kPa or $\sigma_v = 200$ kPa was applied until the end of consolidation was registered.

The program of controlled freezing was the same for all samples and the cooling rate of the coolant was 3°C per hour. After the insulation was placed on the top and sides of the mold the latter was placed on a freezing plate for freezing (*see* Figures 3 and 4).

Directional freezing took place from the base upward which minimized freezing strains and stresses. The freezing process was stopped after reaching the desired test temperature on the top of the sample, and then the sample remained in the cold room at the test temperature for 12 to 24 hours without insulation to get a homogeneous temperature distribution.

All samples were protected against sublimation during the test by a thin rubber membrane or by a layer of grease.

Uniaxial Compression Tests

The tests were performed as creep tests on cylindrical samples with constant creep stress σ_1. The outline of the test equipment is given in Figure 3.

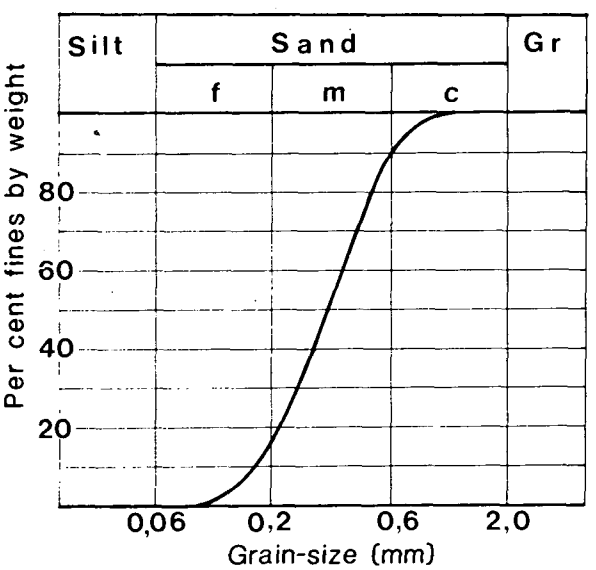

$\gamma_s = 26{,}6$ kN/m^3

min $\gamma_d = 14{,}6$ kN/m^3

max $\gamma_d = 16{,}9$ kN/m^3

FIGURE 1. Properties of sand.

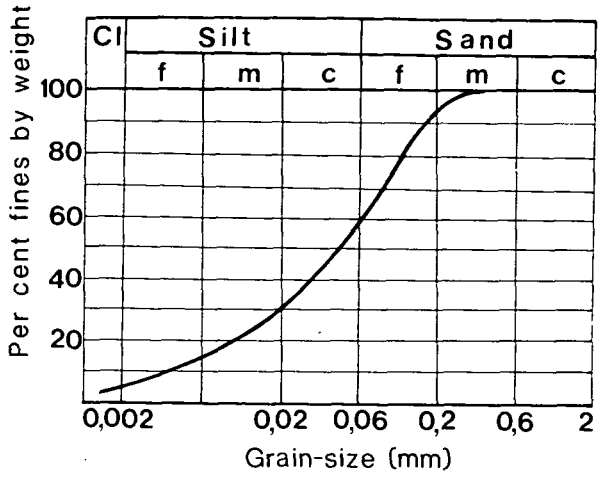

$\gamma_d = 14{,}6$ kN/m^3

$w_l = 34{,}0$ %

$w_p = 19{,}1$ %

$I_p = 14{,}9$ %

FIGURE 2. Properties of silt.

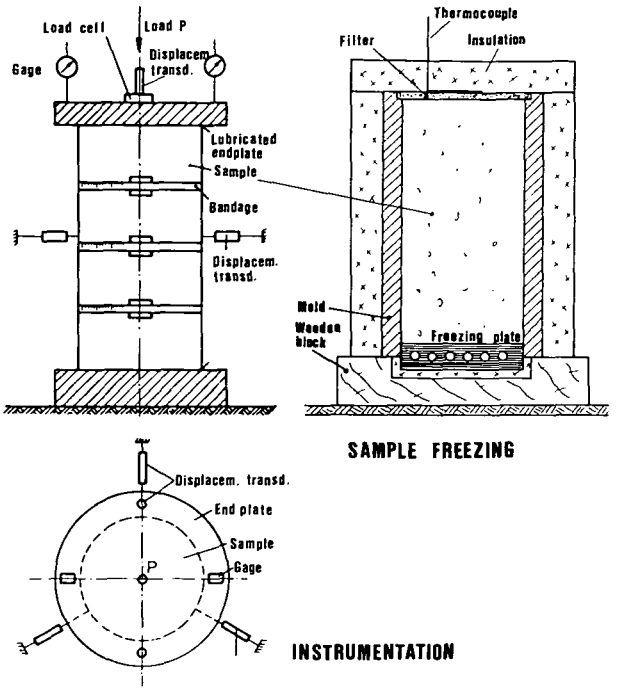

FIGURE 3. Uniaxial compression test.

The load was applied by a hydraulic system with a regulated oil volume per pumping stage. For load registration a strain-gauge load cell within the piston was used. The measured value was compared automatically with a given electrical value corresponding to the desired oil pressure P_H of the hydraulic system, and the oil pump was regulated by the difference of these two values, so that creep load was kept constant. In order to compensate the increase of sample cross section during deformation, a load increase had to be made manually to keep the creep stress σ_1 constant. This load increase was made after attaining a cross section difference of $\Delta F = 1.3$ per cent of the original size. In most of the tests, the creep stress σ_1 was also increased to a higher value after a given time interval.

During the sample loading process, the hydraulic pressure P_H was shown on a manometer and the stress rate $\dot{P}_H$ was held constant for all tests as much as possible with an average value of about $\dot{P}_H = 1000$ kPa/min.

In order to have the possibility of testing undisturbed samples with the same test equipment, the sample dimensions were chosen with height $h = 20$ cm and diameter $d = 10$ cm. A second reason for such a large sample diameter was the mechanical method for measuring the sample circumference during the test. This was done by three plastic strips with a millimetre scale on it, set in the three points along the sample height. For the mechanical measurement of axial deformations two gauges were installed on top of the upper sample end plate. The electrical measurement of deformations was done by displacement transducers. Two were set for vertical, three for horizontal displacement, and the data were recorded by a data logger. The room temperature in each test was measured by thermocouples as well as by thermometers.

The end platens were larger in diameter than the sample and they were lubricated to permit homogeneous sample deformation.

During a test, displacements, load, temperature, and time were recorded and as a result, curves were drawn by means of a computer program.

Uniaxial Tensile Tests

Different kinds of tests exist for the investigation of a material stress-strain behaviour under tension (Frankenstein 1969; Haynes 1973; Offensend 1966). Especially for the investigation of creep behaviour, the simplest test method was found to be the direct tension test under uniaxial stress conditions. By processing test results from those tests, no assumptions concerning the stress-strain behaviour are necessary as it would be in a bending test.

Recently Jessberger (1980) gave a synopsis of speci-

men shapes used for tensile tests with ice and frozen soils. A sketch of sample and test equipment used in the author's tests is given in Figure 4.

The sample was a dog-bone shaped specimen with a cylindrical middle section. Only the middle section with height h = 15 cm and diameter d = 5 cm was used for deformation measurements. In order to be able to test undisturbed samples with the same equipment, the sample diameter was chosen according to the minimum borehole drilling diameter. The length of the sample middle section was selected as a compromise of sample freezing duration, minimum length of an undisturbed sample, and accuracy of deformation measurements.

The radius of the sample end sections was r = 28 cm so that no significant stress concentrations could exist. Hawkes and Mellor (1972) found no significant stress concentrations in their photo-elastic study with a smaller radius r = 7 cm, similar to the ones used by Haynes (1973). The experiences with testing concrete samples, however, showed better results with a larger radius.

The creep load was applied by means of a lever arm. The loading stress rate $\dot{P}_H$ was controlled mechanically and an effort was made to hold it constant and equal to $\dot{P}_H$ = 1000 kPa/min, as in the compression tests, in order to eliminate its influence.

From the lever arm the creep load was transferred to the sample by means of screw rods which were fixed in the sample end platens. These rods with a diameter of d = 3 mm were of different lengths (*see* Figure 4) and the total length of all rods at one specimen end was 50 cm. A later calculation from test results showed an adhesive strength between frozen soil and rods of more than 0.16 kN/cm length.

The end platens were attached in a plane parallel manner on the mold during sample preparation and freezing process. In this way, load eccentricity was kept as small as possible, and was in fact negligible. Sample preparation and freezing processes were the same procedures as for compression tests. The volume increase occurring when water freezes, produced a pre-stressed connection between the screw rods and the frozen material, and this is why there are no problems of load transfer with this technique.

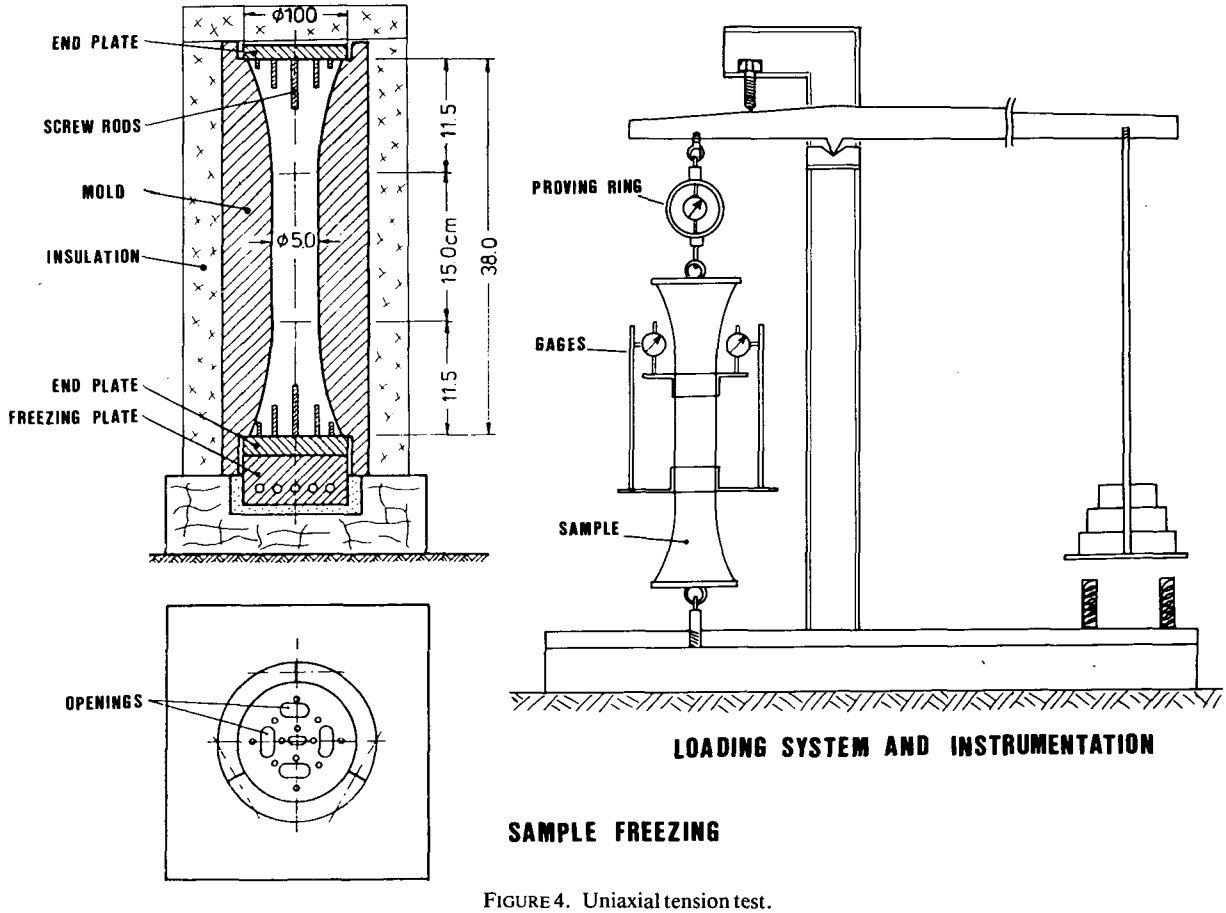

FIGURE 4. Uniaxial tension test.

These tension tests were performed as creep tests with constant creep load instead of constant creep stress σ_1, but as test results later show, there was no great variation of σ_1 within one test caused by the change of sample diameter. After each test, the sample diameter was measured by means of a caliper for the volume control and it was found that the maximum change of sample diameter of about 1 mm caused a maximum stress increase of about four per cent of the initial stress σ_1. This value is within the same order of accuracy as the creep stress regulation in the compression tests.

All deformation and load measurements were done mechanically. The load was measured by a proving ring and for axial deformations two gauges, attached on a special ring, were used (*see* Figure 4). This ring consisted of two halves which were screwed together with pre-stressed screws to guarantee a good seat in case of sample diameter reduction.

As soon as a creep load was applied measurements of deformation, load and temperature were taken as a function of time. The temperature was held constant in each test. The results were plotted as creep curves.

Test results

Compression Tests

As a result of fully automated data recording, creep curves were plotted by means of a computer program.

Figure 5 gives an example of a sand sample deformation as a function of time for constant creep stress σ_1 = 6000 kPa and constant temperature T = −10°C. Curve 1 shows an increase of axial deformation ε_1 with time after load application, and in the first portion, strain rate $\dot{\varepsilon}_1$ is decreasing. After reaching an axial deformation of about ε_1 = 8 per cent, strain rate $\dot{\varepsilon}_1$ increases again, and finally sample failure occurs. Curve 3 shows the same behavior for radial deformation ε_3. The mainly horizontal progress of curve V shows a nearly constant volume deformation ε_v until failure point is reached. This behaviour was found to be typical for all samples including specimens made of clayey sandy silt, as seen in Figure 6.

Figures 7 and 8 give some more results for axial deformation ε_1 of sand samples at temperatures of T = −20°C and T = −30°C. More results for sand samples and different temperatures are published by Eckardt (1979 *a* and *b*). Creep curves from tests with

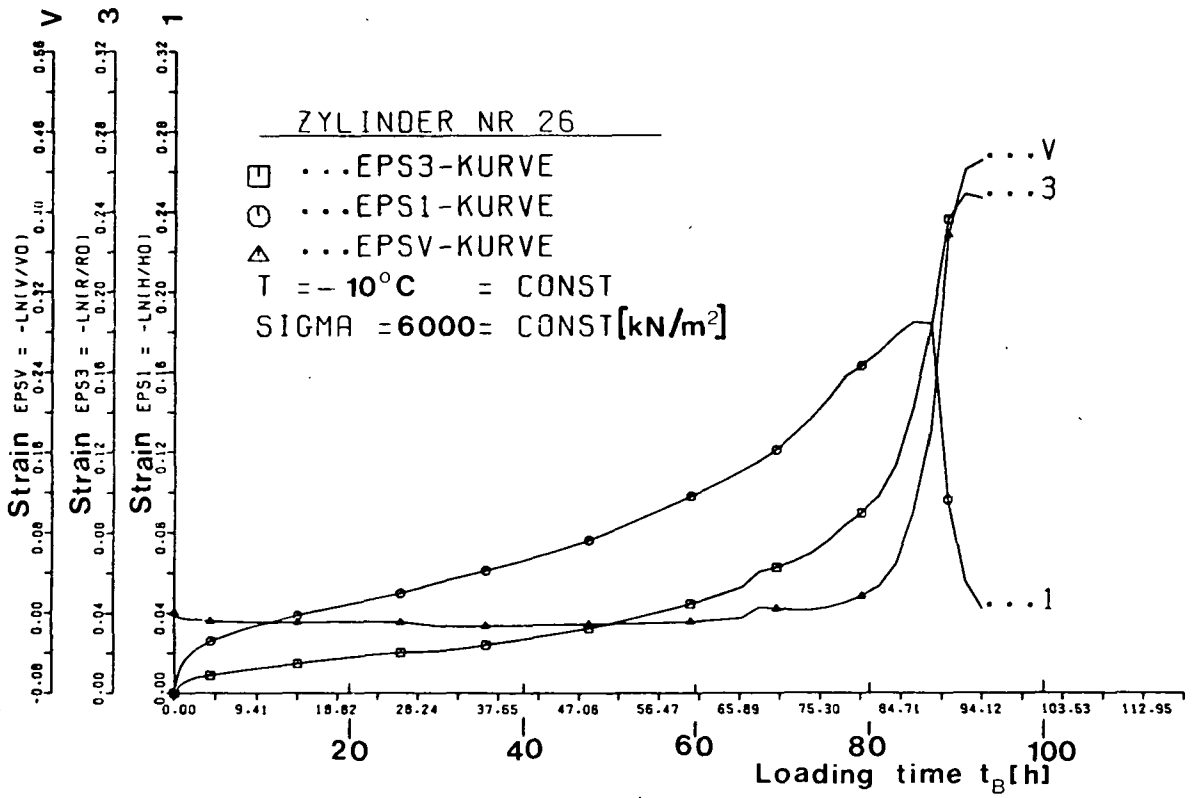

FIGURE 5. Creep deformations; compression test; sand.

undisturbed samples of frozen clayey sandy silt are given in Figure 9 and some more results of tests with a similar soil are published by Meissner and Eckardt (1980).

Most of the samples were stage-loaded in order to reduce the test time and to get as much information as possible about creep behaviour from one sample. In general, test results show an increasing axial sample deformation ε_1 with increasing creep stress σ_1 for the same duration of loading and constant temperature; ε_1 decreases with decreasing temperature T for constant time and constant stress.

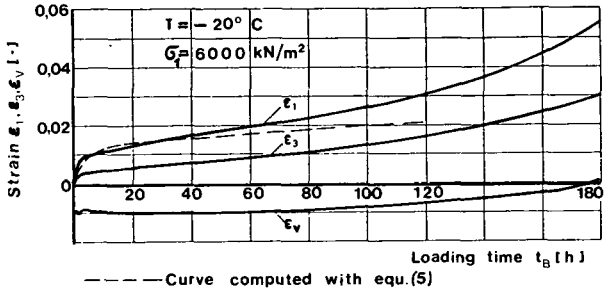

FIGURE 6. Creep deformations; compression test; silt.

Tensile Tests

In tensile tests there was much more dispersion of test results than in compression tests, but obviously all samples under tension showed a different creep behaviour from that under compression under comparable test conditions. Figure 10 shows comparable

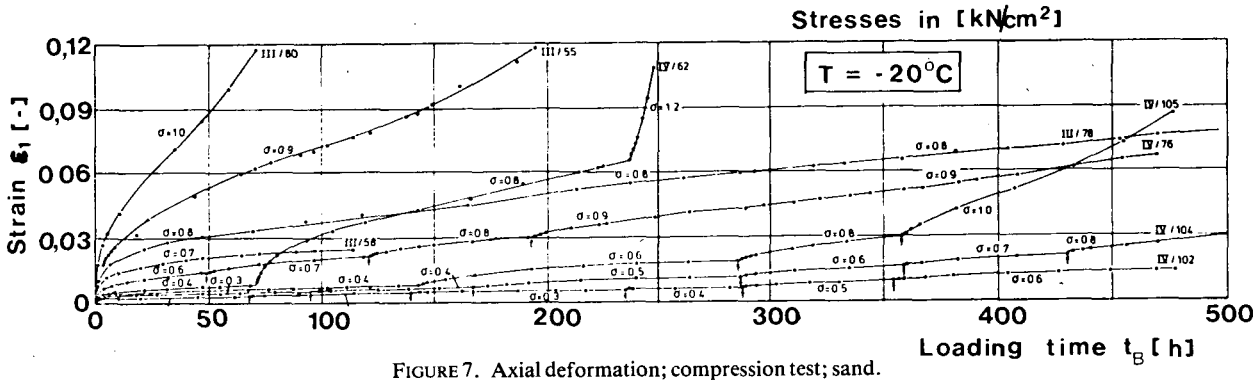

FIGURE 7. Axial deformation; compression test; sand.

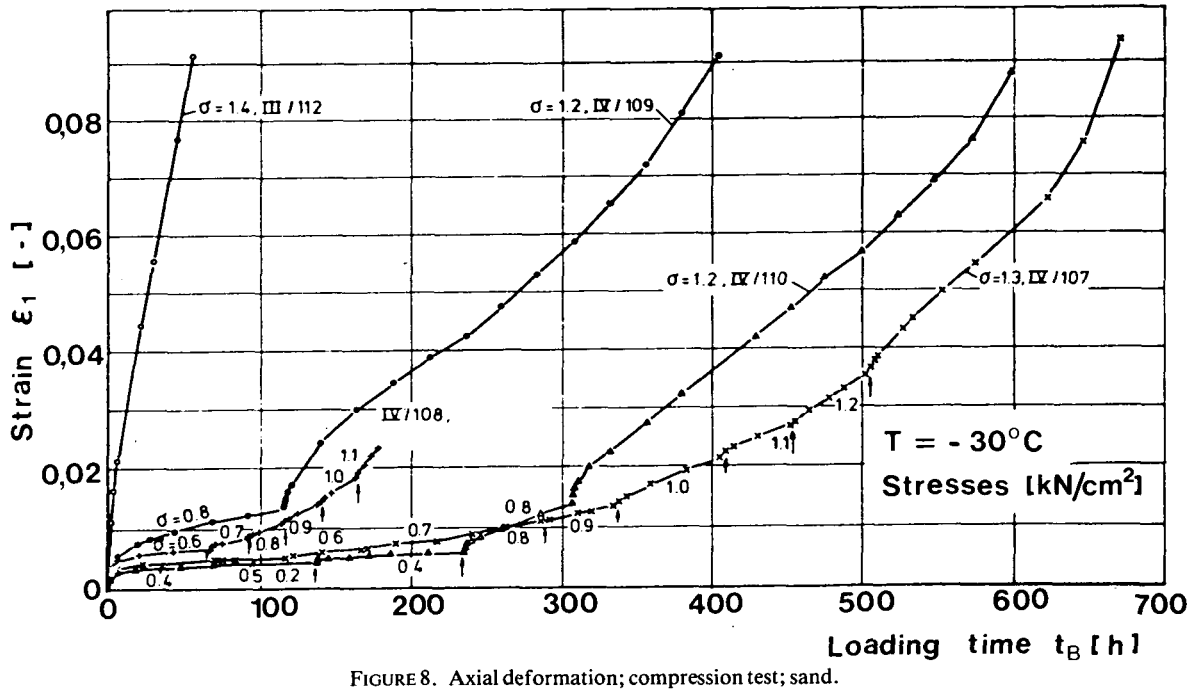

FIGURE 8. Axial deformation; compression test; sand.

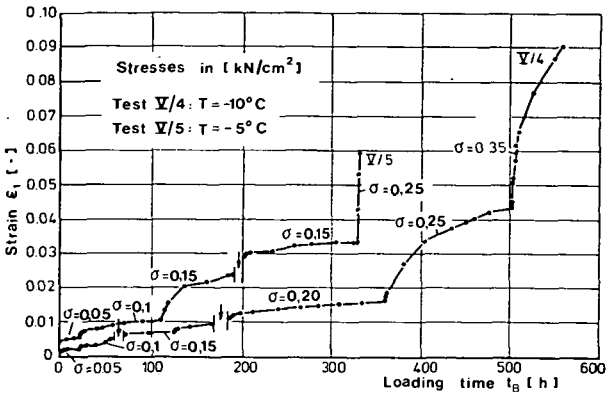

FIGURE 9. Axial deformation; compression test; silt.

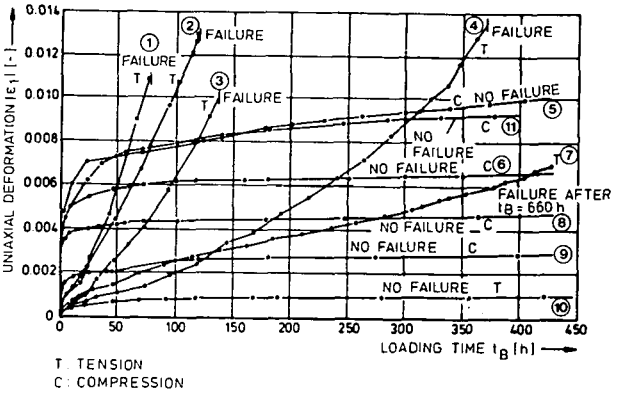

curve Nr	test Nr	load comp./tens.	stress σ1 [kN/cm²]	temp. T [°C]
①	VII/31	T	0.19	-10
②	VII/34	T	0.29	-15
③	VII/32	T	0.17	-10
④	VII/33	T	0.16	-10
⑤	III/86	C	0.30	-15
⑥	III/153	C	0.17	-10
⑦	VII/356	T	0.12	-10
⑧	III/118	C	0.10	-10
⑨	III/119	C	0.05	-10
⑩	VII/37	T	0.05	-10
⑪	III/117	C	0.20	-10

FIGURE 10. Creep curves from uniaxial tests under compression and under tension.

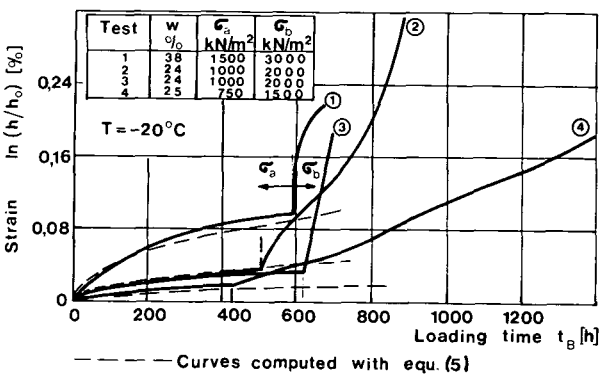

FIGURE 11. Axial deformation; tension test; silt.

creep curves for axial deformation ε_1 of sand samples under compressive and tensile stresses.

At the beginning of load application, axial tensile strains remain far below any comparable compression strains. Also failure deformation under tension is much smaller than under compression. Strain rate $\dot{\varepsilon}_1$ under tension is higher than under compression for medium and high stresses, but it is of the same order of magnitude for low stresses. Further more sand samples under tensile stress were obviously more sensitive to creep stresses σ_1 than samples under compression which means that the range of stresses from zero to the failure stress was much smaller under tension than under compression.

Some results of creep tensile tests on samples from clayey sandy silt are given in Figure 11. Shown are the axial deformations ε_1 after five hours of loading time. The time independent deformations were between $\varepsilon_o = 0.01$ per cent and $\varepsilon = 0.04$ per cent, depending on consolidation stress $\sigma_v = 100$ and 200 kPa during sample preparation and on first creep stress σ_1. In these tests, creep load was increased after a loading time of about 500 to 600 hours to reduce the test time and to find a maximum value of creep load. Within the observed test period, doubling the creep stress σ_1 obviously causes a strain rate $\dot{\varepsilon}_1$ which is more than twice as high as before. The table insert in Figure 11 gives the different tensile stresses before and after load increase, as well as the water content of each sample after the test.

Time-dependent Stress-strain Behaviour

From different creep curves axial deformation ε_1 can be taken for constant time and constant temperature as a function of creep stress σ_1 in compression and tension. As a result one gets the function

$$\sigma_1 = f(\varepsilon_1)$$

As shown in Figure 12 for the medium grain-size sand, the controlling parameters are stress, time, and temperature.

Data for Figure 12 were taken only from the primary and secondary stage of creep, and for all curves the relationships between stress σ_1 and strain ε_1 are non linear. This is also true for cohesive soils. Curves for tensile stresses end at smaller deformations ε_1 than curves for compression because failure strain under tension is much smaller than under compression. As long as failure deformation ε_f under tension is not exceeded, one can apply higher stresses under tension than under compression for the same conditions of loading time t_B, temperature T and deforma-

tion ε_1. In any case, lowering the temperature means that a higher stress can be applied at the same duration of loading and constant strain.

Long-term Strength

At constant temperature, all creep curves show an increase of sample failure time with decreasing creep stresses σ_1. That creep stress, causing the sample failure after an infinite loading time $t_B = \infty$ is called long-term strength σ_∞. From creep curves of compression tests with sand samples, the failure strain ε_f was found to be between six and eight per cent and is assumed to be constant. Similar results of stress and time independent failure deformation can be found in concrete technology (Wittmann and Zaitsev 1974).

Tensile test samples show in general smaller failure deformations than those from compression tests. The large dispersion of test results however does not allow to give a quantitative value. Nevertheless, for further data processing it is assumed to be constant as well.

In Figure 13, creep stress σ_1 is shown as a function of failure time t_{Bf} for those samples where failure occurred because of tertiary creep under constant stress.

The relationship between creep stress σ_1 and failure time t_{Bf} is non-linear for all curves. In general, stress decrease with time is higher under compression than under tension. The relation $\Delta\sigma/\Delta t_{Bf}$ seems to be nearly independent of temperature within the range investigated.

Tension tests show a long-term strength which is about 1/3 to 1/4 of the comparable long-term strength under compression. For the clayey sandy silt the long-term strength under tension is smaller than the one for sand under comparable conditions. This result is typical for frozen cohesive soils. Very similar results were found by Grechishchev (1976). Analytical expressions for describing the long-term strength have been published by Jessberger (1980).

From all tests with frozen sand, the density of the ice matrix was calculated and the computed values were between $\rho_{ice} = 820\,kg/m^3$ and $\rho_{ice} = 910\,kg/m^3$. An average value from the literature for amorphous ice is about $\rho_{ice} = 917\,kg/m^3$ and Hobbs (1974) gives a range between $\rho = 916\,kg/m^3$ and $\rho = 934\,kg/m^3$. The lower result in this paper might have been caused by included air bubbles. A very similar value of $\rho = 904\,kg/m^3$, which is close to the author's test result, was found by Haynes (1973) for a bubbly polycrystalline ice.

Analysis

The analysis should furnish an analytical relationship between stresses and strains. Taking deformation ε_1 as an independent variable it should be possible to predict the corresponding stress σ_1 in a deformed soil sample. For the development of these equations from test results, the following assumptions and restrictions are made:

— the frozen soil is taken as a continuum;
— only uniaxial states of stresses are described;
— all deformations are monotonous;
— the stress path is only of loading type (no unloading);
— the sample volume is assumed to be constant; and
— no tertiary creep is described.

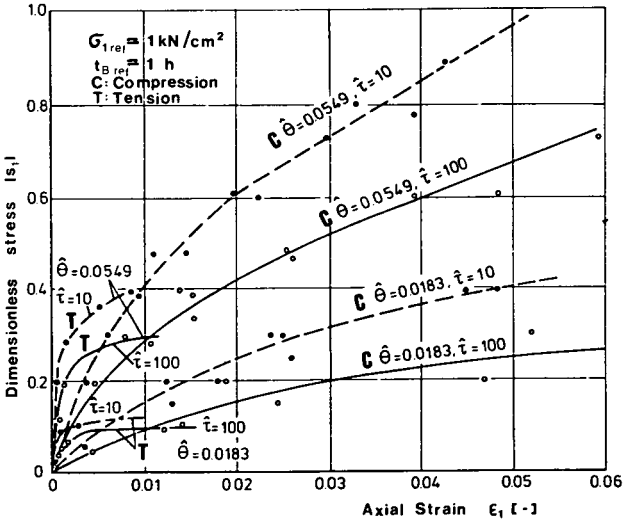

FIGURE 12. Stress–strain curves, sand, compression + tension.

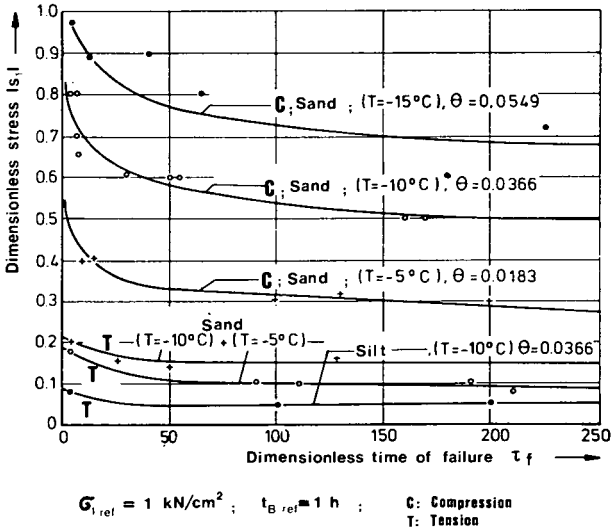

FIGURE 13. Creep strength for sand and silt; compression + tension.

It was found that a good description of creep curves from both compression and tension tests can be given in the form

[1] $\varepsilon_1^m = \sigma_1 \cdot 1/K(T, t_B)$

where ε_1 is the axial deformation, σ_1 the axial creep stress, m is a material constant and K is a parameter dependent on temperature T and loading time t_B.

Taking deformation ε_1 as the independent variable, equation 1 can be written for computing the corresponding creep stress σ_1 as

[2] $\sigma_1 = K(T, t_B) \cdot \varepsilon_1^m$.

From the results of compression and tension tests the modulus $K(T, t_B)$ was found to be

[3] $K = (1 - T)^k \cdot w_o \cdot t_B^{-\lambda}$

with k, w_o, and λ being parameters taken from test results. For a more general purpose, equation 3 can be written in a dimensionless form as

[4] $K = \hat{\theta}^k \cdot \omega_o \cdot \hat{\tau}^{-\lambda}$

with the following definitions:

[4a] dimensionless temperature $\hat{\theta} := \dfrac{T_o - T}{T_o - T_{\omega_o}}$

T_o = melting temperature of ice in any temperature scale
T = test temperature in the same scale as T_o
T_{ω_o} = reference temperature in the same scale as T_o

[4b] dimensionless time $\hat{\tau} := t_B/t_{B_\omega}$

t_B = loading time
t_{B_ω} = reference time

[4c] dimensionless stress $\omega_o := \sigma/\sigma_{ref}(\hat{\tau}, \hat{\theta}, \varepsilon_\xi)$

σ = creep stress
σ_{ref} = reference creep stress
$\hat{\tau}, \hat{\theta}, \varepsilon_\xi$ = chosen values of time, temperature, and deformation.

A complete derivation of equation 4 has been published by Eckardt (1979*b*) and is briefly repeated in the Appendix. With equation 4 one can write a dimensionless form of equation 2 as

[5] $s = \hat{e}^m \cdot \tau^{-\lambda} \cdot \hat{\theta}^k \cdot \omega_o$

with definitions of

$s := \sigma_1/\sigma_{ref}$ dimensionless uniaxial stress

[5a] and

$\hat{e} := \varepsilon_1/\varepsilon_\xi$ uniaxial deformation.

In general, equation 5 holds for both investigated frozen soils under compression and tension, but the different material behaviour leads to different parameters in tension tests and in compression tests. For the medium grain-size sand a complete calculation of parameters is given by Eckardt (1979*b*), and the average values of the parameters are given in Table 1.

TABLE 1. Average values of parameters for medium grain-size sand

Compression	Tension	Reference values
$m_c = 0.62$	$m_t = 0.20$	$\sigma_{ref} = 1\,kN/cm^2\,(\hat{=}\,10\,MPa)$
$\lambda_c = 0.16$	$\lambda_t = 0.11$	$t_{B\,ref} = t_{B_\omega} = 1\,h$
$\omega_{oc} = 210$	$\omega_{ot} = 24$	$T_{ref} = T_{\omega_o} = -273,15°C$
$k_c = 1$	$k_t = 1$	$\varepsilon_\xi = 1$

Computed creep curves with these parameters and using equation 5 are shown in Figure 14.

The calculated curves in general show the same tendendy as creep curves from tests (*see* Figure 10). For a good accuracy of calculated results it is recommended to evaluate the parameters of equation 5 from those tests which have the same ranges of stress, strain, temperature, and time as in the particular practical problem.

For clayey sandy silt, average values of the parameters were evaluated (Table 2). Computed creep curves for tension tests are compared with test results (*see* Figure 11). Curve of test Z 56S does not fit as well as the other ones but this might be due to the water content of this particular sample, which was different from the others.

The given values for sand are more different for compression and tension than those for clayey sandy silt. The presented data are still too few to predict the parameter development as a function of the grain-size distribution. Also by means of parameter values from the literature (Andersland and Anderson, 1978,

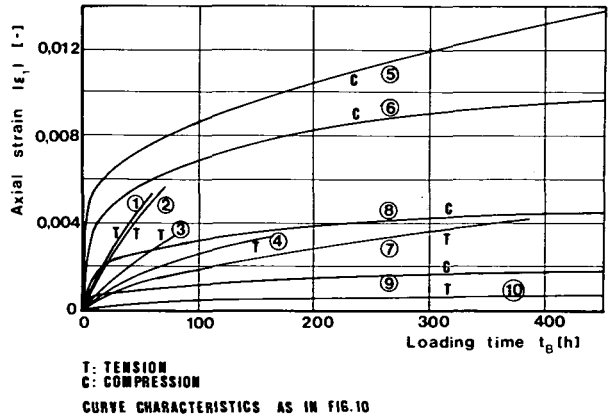

FIGURE 14. Creep curves for sand; compression + tension, computed with equation 5.

p. 233) no clear tendency can be found. This shows the difficulty, even today, to find exact parameters for a given practical case even if the boundary conditions of the test are well defined. Meissner and Eckardt (1980) have shown how the parameter values can differ for the same soil if stress and temperature history are taken into account or not.

TABLE 2. Average values of parameters for clayey sandy silt

Compression	Tension	Reference values
$m_c = 0.70$	$m_t = 0.43$	$\sigma_{ref} = 1\,kN/cm^2\,(\hat{=}\,10\,MPa)$
$\lambda_c = 0.14$	$\lambda_t = 0.19$	$t_{B\,ref} = t_{B_\omega} = 1\,h$
$\omega_{oc} = 250$	$\omega_{ot} = 140$	$T_{ref} = T_{\omega_o} = -273,15°C$
$k_c = 1$	$k_t = 1$	$\varepsilon_\xi = 1$

Discussion

It is obvious that creep behaviour differs under tension and compression, specially for sand. This might be an indication for the effect of the grain skeleton on creep behaviour. The influence of the grain skeleton on shear strength is shown by Goughnour and Andersland (*in* Andersland and Anderson 1978, p. 255). They found an increase of axial peak stress with an increase of volume concentration of Ottawa sand in frozen sand samples. Pusch (1979) found also that, in creep of Emscher marl, the particle network has some reinforcing effect, because the creep rate of this clayey silt at low and intermediate stresses was considerably lower than that of ice.

The same phenomenon can also be observed in testing of concrete samples or samples of cement stone. For this material, that phenomenon can be described by means of the modified equation of Einstein viscosity (Reiner 1968). But, as shown by Eckardt (1979*b*), this equation does not yield acceptable results for frozen soils.

After Pusch (1979) there are three, main, damaging processes which may take place in the course of creep. They are

— pressure- and strain-induced heat production;
— slip along crystal interfaces; and
— formation of slip-bands, fissures, and cracks.

Recrystallization is probably the main healing mechanism in creep. With these main mechanisms an explanation of the different creep behaviour under compression and under tension might be possible. In the case of tensile stresses, no transfer of normal stresses by means of the grain skeleton is possible. Only the ice matrix is able to transfer tensile stresses. In case of compression at points of high stress concentrations, the ice will melt and new points of intergranular contact will arise. The melted ice will refreeze and so the creep process slows down as long as the loss of ice-bearing capacity is compensated by an increase of number of intergranular contacts. Otherwise tertiary creep will start. In the case of tension, cracking will occur if the tensile strength of ice is exceeded. Crack length can be limited by a sand grain but the cracked cross section does not give any further contribution to the stress transfer.

The reinforcing effect of the grain skeleton might not be the only reason of the higher viscosity of frozen sand samples compared with ice. Another physical explanation might be given in the different ice growing conditions in both materials. Because of different thermal conductivity of quartz sand and water it can be assumed that in frozen soils the freezing process starts around a sand grain. This process produces ice crystals of different orientation and, as a consequence, the ice structure in frozen soil samples is different from that in pure ice samples with heat transfer in vertical direction. In this case, ice crystallisation occurs in a hexagonal shape with C-axis in freezing direction (Hobbs 1974). Creep behaviour of pure ice is therefore anisotropic. It is assumed by the author that the modified irregular ice structure in a frozen soil sample has a higher creep strength than that in pure ice samples. This idea that orientation of ice crystals might have an effect on creep behaviour is supported by test results from Dykins (1969) who found that "grain (crystal) size had little effect on strength; however, the orientation of the grain and sub-grain structure in relation to the stress orientation had an appreciable effect". For time-independent properties of ice there are some values reported from Michel and Lafleur (1977) which are provided here in Table 3.

TABLE 3. Values for time-independant properties of ice

	Columnar ice horizontal *C*-axis size of grains: 12.5 mm $\rho = 911\,kg/m^3$	Columnar ice SI monocrystalline direction of loading 45° with the *C*-axis
Compression *strength:*	$\sigma_c = 4530\,kPa$	$\sigma_c = 16{,}800\,kPa$
Tensile strength:	$\sigma_t = 1350\,kPa$	$\sigma_t = 2230\,kPa$
Shear strength:	$\tau = 1020\,kPa$	—

Source: Michel and Lafleur (1977).

As one can see, the orientation of the crystal *C*-axis to the direction of loading influences the compressive and tensile strengths very strongly. The compression strength is about four times higher and the tensile strength about two times higher for ice loaded under an angle of 45° measured against the *C*-axis. Similar

differences for compressive strength of ice depending on direction of the *C*-axis were also reported by Jumikis (1966).

A better explanation of the different creep behaviours of frozen soils, and also a better assessment of the presented test results, might be possible if more information about the micro-structure, the main displacement processes within a sample, and about the influence of stress- and temperature history on the form and size of the ice crystals becomes available. Interesting progress in that direction has been made by Pusch (1979), who developed a simple tension stage for microscopic study of the deformation of frozen soils and ice.

All tests reported in this paper were performed under uniaxial states of stress and, as mentioned earlier, the results are restricted to those states of stress. But, in practice, it is necessary to describe also more-complex states of stress. As equation 1 is an engineering approximation of test results and not a theoretically based material law, its generalization should be handled with care. Nevertheless, a generalization of equation 1 to a scalar deviatoric equation in form of

$$\varepsilon_1 - \varepsilon_2 = K(T, t_B)(\sigma_1 - \sigma_2)^{\alpha}$$

where $\varepsilon_1, \varepsilon_2, \sigma_1, \sigma_2$ mean the components of strain and stress ($\sigma_1 > \sigma_2$), might be possible and was used by Winter (1980) for shaft creep calculations. For a better understanding and description of creep behavior of frozen soils under multiaxial states of stress, triaxial tests are now underway and the first results are being prepared for publication. For strain rates $\dot{\varepsilon}_1$ higher than in normal creep, some test results have been published by Sayles (*in* Andersland and Anderson, 1978, p. 252).

For creep tensile tests under triaxial conditions, first results were published by Jessberger (1980) but they are still too few for developing an analytical expression for the description of test results.

Acknowledgements

This paper was written during the author's stay at the Northern Engineering Centre of Ecole Polytechnique (CINEP) in Montréal, Canada. The financial support by CINEP and by NATO, given through the German Academic Exchange Service (DAAD) is greatfully acknowledged.

References

ANDERSLAND, O.B. AND ANDERSON, D.M., (Eds.). 1978. Geotechnical Engineering in Cold Regions, McGraw-Hill Book Company, 566 p.

CHAMBERLAIN, E., GROVES, C., AND PERHAM, R. 1972. The mechanical behaviour of frozen earth materials under high pressure triaxial test conditions. Geotech., vol. 22, no. 3, pp. 469–483.

DYKINS, J.E. 1969. Tensile and Flexure Properties of Saline Ice. Proc. Int. Symp. Physics of Ice, Munich, West Germany, September 1968, Plenum Press, New York. pp. 263–271.

ECKARDT, H. 1979*a*. Creep behavior of frozen soils in uniaxial compression tests. Eng. Geol., vol. 13, pp. 185–195.

_____. 1979*b*. Tragverhalten gefrorener Erdkoerper. Publ. Inst. Soil Mech. and Rock Mech., Nr. 81, University of Karlsruhe, West Germany, 141 p.

FRANKENSTEIN, G.E. 1969. Ring Tensile Strength Studies of Ice. CRREL, Hanover, N.H., USA, Tech. Report 172, 78 p.

GRECHISHCHEV, S.E. 1976. Basis of Method for Predicting Thermal Stresses and Deformations in Frozen Soils. Natl. Res. Counc. Can., NRC/CNR-TT 1886, Transl. 228 for the Div. Build. Res. Ottawa.

HAWKES, J. AND MELLOR, M. 1972. Deformation of Fracture of Ice under Uniaxial Stress. J. Glaciol., vol. 11, no. 61. pp. 103–131.

HAYNES, F.D. 1973. Tensile Strength of Ice under Triaxial Stresses. Cold Regions Res. Eng. Lab., Hanover, N.H., Research Report 312. p.

HOBBS, P.V. 1974. Ice-Physics. Clarendon Press, Oxford, 837 p.

JESSBERGER, H. 1980. State-of-the-Art Report ground freezing: Mechanical Properties, Processes and Design. Proc. 2nd Int. Symp. on Ground Freezing, Trondheim, Norway, pp. 1–33.

JUMIKIS, A.R. 1966. Thermal Soil Mechanics. Rutgers Univ. Press, New Brunswick, 54 p.

MEISSNER, H. AND ECKARDT, H. 1980. Materialkenwerte gefrorener Boeden. Die Bautech., no. 11, pp. 388–391.

MICHEL, B. AND LAFLEUR, P. 1977. Mechanical Properties of Natural Ice to Impact loading. Report T-20, Univ. Laval, Québec, Canada.

OFFENSEND, F.L. 1966. The Tensile Strength of Frozen Soils. CRREL, Hanover, N.H., USA, Technical Note.

PUSCH, R. 1979. Creep of Soils. Schriftreihe des Inst. fuer Grundbau, Wasserwesen und Verkehrswesen, Serie Grundbau, No. 5, Ruhr — Univ. Bochum, 76 p.

REINER, M. 1968. Rhéologie in elementarer Dartellung. Carl Hauser-Verlag, 360 p.

SAYLES, F.H. 1968. Creep of Frozen Sands. CRREL, Hanover, N.H., USA, Techn. Report 190.

WINTER, H. 1980. Creep of frozen Shafts: A Semi-Analytical Model. Proc. 2nd Int. Symp. on Ground Freezing, Trondheim, Norway, pp. 247–261.

WITTMANN, F. AND ZAITSEV, J. 1974. Verformungen und Bruchvorgang poroeser Baustoffe bei kurzzeitiger Belastung und Dauerlast. Dtsch. Ausschuss fuer Stahlbeton, Nr. 232, Berlin, West Germany, 168 p.

ZELENIN, A.N., VESELOV, G.M., AND STEPANOV, A.P. 1958. Results of laboratory Tests on Strength Behavior of Frozen Soils. (*in Russian*). Mosk. Bergbauinst. Akad. Wiss., USSR, Verlag Igletechizdat, Moskow, 48 p.

Appendix

Derivation of equation 4:

The modulus K in equation 1 is assumed to be dependent on time t_B and temperature T. For a more general purpose K can be written in a dimensionless form as

[6] $\quad K = K(\theta,\tau).$

The definition for θ is

[7] $$\theta := \frac{T_o - T}{T_o - T_{ref}}$$

where T_o and T are of the same meaning as in equation 4a and T_{ref} is an arbitrary reference temperature. τ is defined by

[8] $$\tau := t_B / t_{B_{ref}}$$

where t_B is the time under load and $t_{B_{ref}}$ an arbitrary reference time.

The function $K(\theta,\tau)$ was obtained graphically by plotting the non linear stress-strain relationship of a frozen soil in a log σ — log ε — plot with τ and θ as the controlling parameters. In this plot the stress-strain behaviour can be approximated by straight lines with the slope m which is assumed to be independent of τ and θ. This is also valid, if σ is replaced by s, defined in equation 5a. In this log s — log ε — plot the modulus $K(\theta,\tau)$ at an arbitrary reference deformation ε_ξ is defined as

[9] $$\xi := s(\tau, \theta, \varepsilon_\xi).$$

Usually ε_ξ is taken as $|\varepsilon_\xi| = 1$.

In order to find $\xi(\tau)$ values of ξ were taken from a log s — log ε plot for different times τ and different temperatures θ at ε_ξ = constant. For constant values of θ these data were approximately connected by straight lines in a log ξ — log τ plot and these lines were nearly parallel to each other with a slope $\lambda = \Delta \ln \xi / \Delta \ln \tau$. The lines are described by

[10] $$\xi = (\tau_\omega / \tau)^\lambda \cdot \omega(\theta)$$

where τ_ω is an arbitrary reference time (usually $\tau_\omega = 1$ hour) and ω is defined by

[11] $$\omega := \xi(\tau_\omega, \theta) = s(\tau_\omega, \theta, \varepsilon_\xi).$$

The function $\omega = \omega(\theta)$ was obtained by taking values of ω at τ_ω = constant for different temperatures θ. In a log ω — log θ plot these values were approximated by a straight line which is described by

[12] $$\omega = (\theta / \theta_\omega)^k \cdot \omega_o$$

where k is the slope of the curve and ω_o is defined by

[13] $$\omega_o := \omega(\theta_\omega)$$

θ_ω is an arbitrary chosen reference temperature, usually taken as $\theta_\omega = 1$.

With equations 12 and 10, ξ is given as

[14] $$\xi = (\tau_\omega / \tau)^\lambda \cdot (\theta / \theta_\omega)^k \cdot \omega_o$$

and with equations 4a, 4b, 7, and 8 it follows that

[4] $$K = \hat{\theta}^k \cdot \omega_o \cdot \hat{\tau}^{-\lambda}.$$